Investigation of Ultra-fast Processes with High Harmonic Generation

Tomas Meerwijk
5731496

July 1, 2020

Electron dynamics are on the order of picosecond to sub-femtosecond timescales. In order to probe these measurements, a sub-femtosecond resolution is required. This can be achieved with spectroscopic measurements which utilize lasers with femtosecond to attosecond pulses. In this report, x-ray excited optical luminescence with high harmonic generation as the excitation source is investigated as a means to measure the timescales of internal conversion in organic molecules and charge transfer from a zirconium oxo cluster to a fluorescent ligand. The results from the investigation of the internal conversion process revealed that XUV excited luminescence is accelerated compared to DUV excited luminescence. This is attributed to quenching due to the charging of the environment as a results of ionizing XUV photons. The investigation on the charge transfer process revealed that the luminescence originates from the zirconium oxo cluster instead of the fluorescent ligand. Further investigation into the internal conversion and charge transfer timescales require measurements on a shorter time range. This requires further optimization of the experiment setup.

1 Introduction

Understanding ultrafast physical and chemical processes such as electron dynamics and chemical kinetics is essential for achieving progress in technology and furthering the knowledge of fundamental processes.[1] To probe these processes, spectroscopic measurements can be performed. The faster the investigated process, the higher the required temporal resolution of the measurements.[2] Electron dynamics are on the order of femtoseconds and therefore require lasers with femtosecond or shorter pulses.[3] In the past fifty years, the temporal resolution has significantly increased due to the shift from picoseconds to sub-femtoseconds laser pulses. The shortest pulse recorded to date being 43 attoseconds.[4]

A novel method for generating sub-femtosecond pulses is high harmonic generation (HHG). Pulses generated by HHG extend into the extreme ultra-violet (EUV) or even soft X-rays, depending on the generation medium. This allows for the use of HHG as a source in experiments involving high energetic transitions, such as edge excitation.[5] X-ray excited optical luminescence (XEOL) is a technique with which a luminescent material is illuminated with X-ray photons and the subsequent visible luminescence is collected. By recording the luminescence intensity as a function of time, information about the temporal aspect of the luminescence can be obtained. Temporal aspects include the lifetime of the luminescence and the rate at which the luminescent state is populated.[6] For these measurements, a

synchrotron is often used as the source of radiation.[7] This requires transport of the sample and set-up to the location of the synchrotron. A tabletop X-ray source gives the ability to perform measurements without having to go to a synchrotron, thereby saving time and money. HHG is such a source which can be incorporated into a tabletop set-up. An alternative to time resolved XEOL for measuring ultrafast processes is transient absorption spectroscopy (TAS). This technique requires finely tuned spatial and temporal overlap of the pump and the probe pulse which is time consuming and can be easily lost.[8] Therefore, due to its facile set up, time resolved XEOL in a tabletop setup with HHG as the excitation source is preferred over transient absorption spectroscopy.

There are relatively few reported XEOL experiments using a tabletop set-up with HHG as the excitation source. It has been reported that this method has been used to investigate the core-valence luminescence In cesium bromide, cesium chloride and barium fluoride.[9] The XUV photons generated by HHG were used to excite core electron to the conduction band, which requires energies between 17 and 22 eV. These experiments have shown that HHG can be used as an excitation source, but did not utilize the temporal properties of HHG. Later, the same group also reported experiments that utilized the high energetic photons as well as the short pulses obtained by HHG. Similar to the previous experiments, CsBr was excited by ultrashort XUV pulses generated with HHG.[10] The resulting luminescence was temporally overlapped with the fundamental beam. By recording the intensity of the resulting difference frequency generation, the lifetime of the core-valence transitions could be determined.

During this internship a tabletop XEOL set-up with HHG as the excitation source was used to investigate ultrafast processes. The focus was on investigating the timescales of internal conversion and charge transfer which are on the order of a few femtoseconds to sub-femtosecond. With internal conversion, the rate at which the luminescent state is populated can be determined. By exciting with DUV and XUV photons this rate can be different, due to the generation of high energetic photons when exciting with XUV photons, which can induce additional processes. The time resolved luminescence can reveal the time scales of the involved processes thereby elucidating the fluorescence mechanisms. The timescale on which a charge is transferred from one system to another is related to the electron mean free path[11] which is important for applications in nanolithography. Line edge roughness and secondary electron blur are consequences of secondary electrons generated by exposing the photoresist with XUV photons.[12] The scale of these processes are dependent on how far the generated secondary electrons can travel, this is related to the electron mean free path.[13] By understanding and eventually controlling charge transfer processes, the secondary electron blur and line edge roughness can be understood and controlled.[14]

In the first part of this report the theory will be discussed concerning luminescence measurements as a means to investigate internal conversion and charge transfer processes and the difference between DUV and XUV excitation. Additionally, a semi-classical description will be given on the HHG process. The second part will be used for describing the methods. This includes the methods for preparing the samples, the experimental set-up, as well as a description of the formulas used for analyzing the data. The obtained results will be presented and discussed in the subsequent part followed by the conclusions.

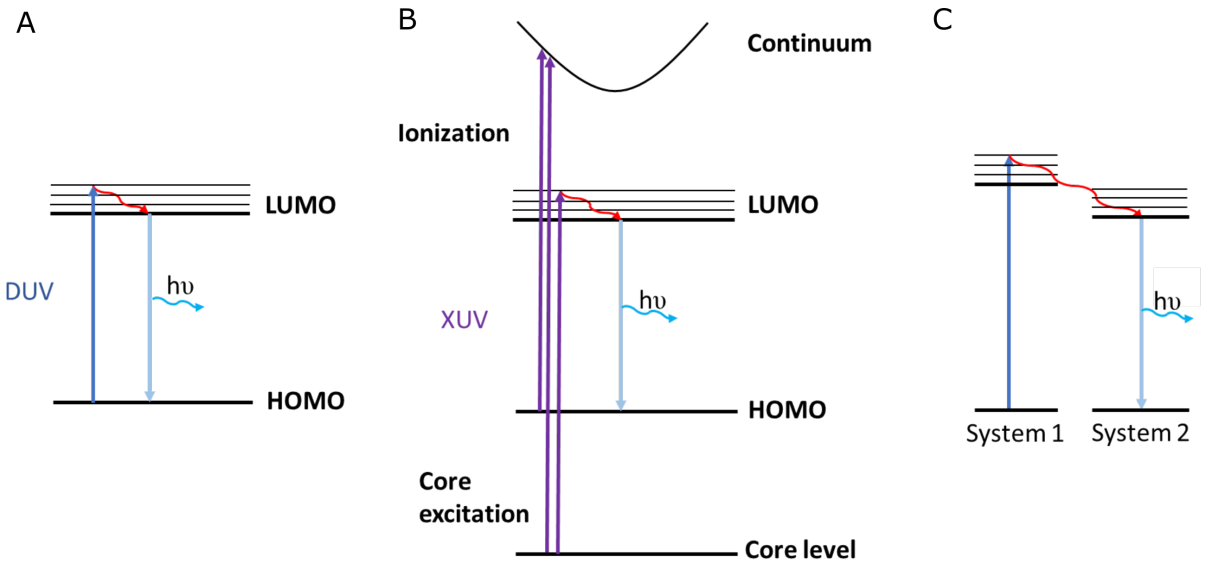

Figure 1: Schematic representations of the energy level diagram corresponding to (A) internal conversion under DUV excitation, (B) internal conversion under XUV excitation and (C) charge transfer under DUV excitation.

2 Theory

2.1 From DUV to XUV excited luminescence

Many materials have the property of emitting light under illumination of higher energetic light. This process called luminescence can tell a lot about the electronic structure of a material. For the luminescence measurements, an excitation pulse is used to bring the material in an energetically higher state. When the system is excited, it will decay back to the ground state by releasing the acquired energy in the form of heat and photons.[15] Important details of the fluorescence are the time it takes for the luminescence to reach its maximum after excited by the higher energetic light, the decrease in intensity as time progresses and the emission wavelength. The time for the luminescence to reach its maximum, also called the rise time, can give an indication about the rate at which the luminescent state is populated. It is important to note that there will always be a finite measured rise time due to the response of the system, so processes that are on the order of the system response time are not reliable. The rate at which the luminescence decreases in intensity and the emission wavelength are characteristic of the investigated material, but can depend multiple factors. These factors are whether the material is a solid or dissolved, the surrounding molecules, the excitation wavelength and the temperature.[16]

Internal conversion involves the processes that take place in order for the excited electron to return to the LUMO after excitation. By exciting the material with light which energy is slightly higher than the energy of the HOMO to LUMO transition (figure 1A) an almost instantaneous population of the luminescent state is expected. The electron is excited from the HOMO to a vibrational excited state of the LUMO followed by non-radiative decay to the lowest vibrational state of the LUMO. The electron then returns to the HOMO with emission of a photon. Exciting the same material with XUV photons induces additional processes (figure 1B). With XUV photons all electrons between the HOMO and the 1s

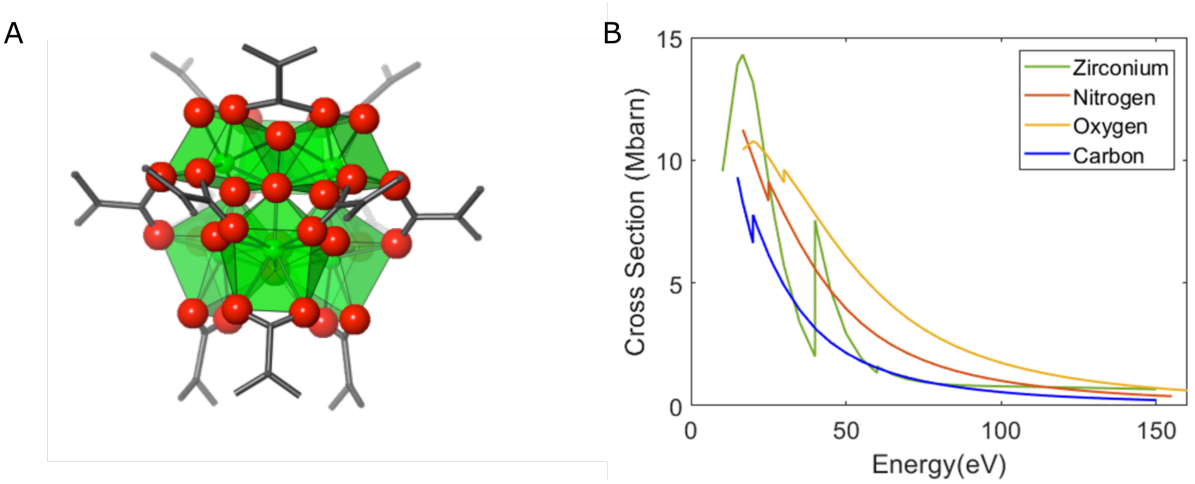

Figure 2: (A) Schematic representation of the Zirconium oxo cluster stabilized with methacrylate ligands, adapted from ref [25]. (B) Absorption cross sections for the elements present during the measurements. Figure generated with data obtained from ref [26].

orbital can be excited to either higher lying energy levels or the continuum, resulting in ionization of the material. The resulting high energetic photons can release its energy by exciting other electrons. By consecutive release of energy, the electron end up at the luminescent state and return to the ground state by emission of a photon. For these measurements, two materials will be investigated: sodium salicylate and 4-(9H-carbazole-9-yl)benzoic acid (4CB). Sodium salicylate is a widely used vacuum ultra violet (VUV) radiation detector.[15] When illuminated with radiation with a wavelength between 30 nm and 350 nm the material shows fluorescence centered around 420 nm with a nearly constant quantum efficiency.[17, 18, 19] The fluorescence matches well with the spectral response of commonly used detectors.[20, 21, 17, 22] Additionally, sodium salicylate is also easily available with low cost. 4CB is a carbazole containing compound which shows fluorescence around 450 nm.[23, 24]

The time resolved luminescence can also be used to investigate the time scales of charge transfer processes. This is possible by combining a fluorescent material with a another material with a large absorption cross section. By tuning the excitation wavelength such that the latter material is excited and observing the luminescence from the fluorescent material, information about the charge transfer process can be obtained (figure 1C). The rise time of the luminescence is indicative of the time it takes for the charge to be transferred from the excited material to the luminescent material. To investigate the charge transfer process, XEOL measurements on a zirconium based photoresist have been performed. The photoresist is a zirconium oxo cluster (ZrOxo cluster) stabilized with 12 methacrylate ligands ($Zr_4O_2(OMc)_{12}$), a schematic representation is shown in figure 2A. To observe the charge transfer process, one or multiple of the methacrylate ligands can be exchanged by 4CB ligands.[25] Due to the abundance of zirconium and oxygen, the absorption cross section (figure 2B) of the ZrOxo cluster is higher than for the 4CB ligand. Therefore, absorption of the excitation beam is expected to occur at the ZrOxo cluster followed by luminescence from the 4CB ligand.

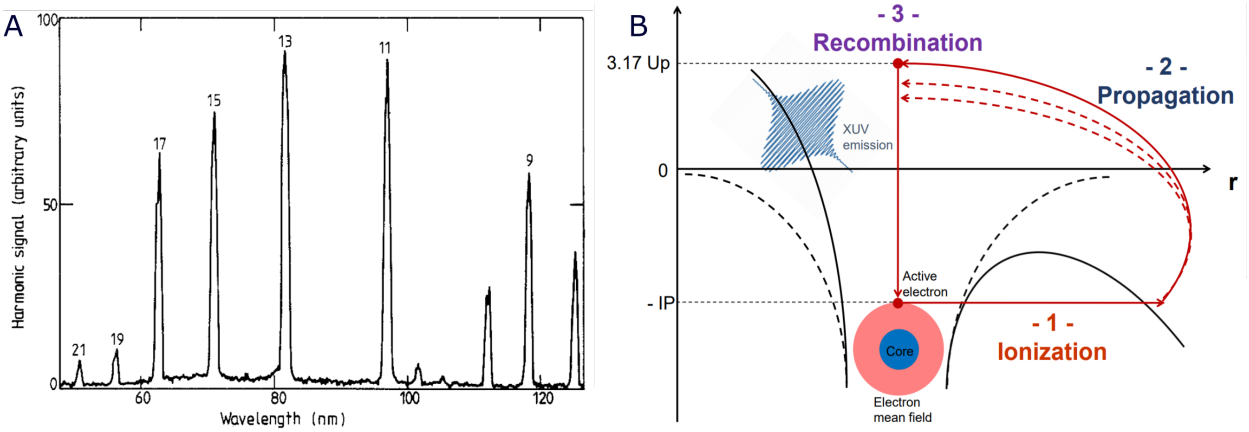

Figure 3: (A) HHG spectrum obtained by generating in Xenon gas with a 1064 nm laser, adapted from ref [28].(B) Schematic representation of the semi-classical three step model description of the HHG process, adapted from ref [13].

2.2 High Harmonic Generation

In order to probe ultrafast processes, light pulses shorter than the rate of the process are required. The processes, which are on the order of fs to as, therefore require ultrashort laser pulses. With commercially available lasers laser pulses of a few tens of fs are easily achieved. Shorter laser pulses require a relatively new technique High Harmonic Generation (HHG). In standard non-linear optics, the efficiency of higher order generation of the fundamental laser pulse scales with the inverse of the order of the process. This means that generating the third order of an 800 nm laser pulse through third order generation is much less efficient than generating the second order.[27] With HHG the efficiency is not dependent on the order and therefore allows a high photon yield at high harmonic orders. One of the first HHG spectra (figure 3A) obtained by focusing ps pulses with a wavelength of 1064 nm into a gas jet with low pressure Xenon gas[28]. The intensity at the gas jet was approximate $3 * 10^{13}$ W/cm^2. The spectrum shows well defined peaks for the 9^{th} up to the 17^{th} order of the fundamental 1064 nm laser pulse. Peaks at higher order energies are also visible, however these are significantly decreased in intensity. The pulses generated by this technique are also much shorter than the length of the fundamental pulse, due to the fact that the HHG process depends quadratically on the electric field strength of the incoming pulse. In the next section the HHG process will be described using the semi-classical three step model as described by Corkum et. al. in 1993[1].

The generation of higher order harmonics of the fundamental laser beam can be described in three steps: Ionization, Propagation and Recombination. An atom, often a noble gas atom, is ionized by the fundamental laser pulse thereby generating an electron in the continuum. The energy of the photons in the fundamental pulse are often below the ionization potential of the atom, therefore the atom is ionized differently. The intensity of the laser beam is strong enough to alter the coulomb potential between the electron and the core thereby allowing electron to tunnel away from the core and entering the continuum (figure 3)B. When the electron is in the continuum it is being propagated by the electric field of the laser. The

electric field induced propagation of the electron can be described by Newtons second law.

$$F_L = -e \cdot E = m_e \frac{d^2x}{dt^2} \tag{1}$$

With E the electric field of the laser.

$$E(t) = E_0 \cos(\omega_0 t) \tag{2}$$

This can be written into the differential equation:

$$\frac{d^2x}{dt^2} = -\frac{e}{m_e} E_0 \cos(\omega_0 t) = -E_0 \cos(\omega_0 t) \tag{3}$$

since $\frac{e}{m_e}$ is a constant, it can be left out for simplicity. This differential equation can be solved analytically. The velocity of the electron can be determined By integrating over time from t_0 to t, with t_0 the time of ionization.

$$\frac{dx}{dt} = -\frac{E_0}{\omega_0}(\sin(\omega_0 t) - \sin(\omega_0 t_0)) \tag{4}$$

The position of the electron can be determined by again integrating over time from t_0 to t.

$$x(t) = \frac{E_0}{\omega_0^2}(\cos(\omega_0 t) - \cos(\omega_0 t_0) + \omega_0 (t - t_0)\sin(\omega_0 t_0)) \tag{5}$$

The last step is recombination. The time of recombination can be determined by finding the roots to equation 5:

$$x(t_r) = \frac{E_0}{\omega_0^2}(\cos(\omega_0 t_r) - \cos(\omega_0 t_0) + \omega_0 (t_r - t_0)\sin(\omega_0 t_0)) = 0 \tag{6}$$

This yields pairs of ionization and recombination times related to the numerically determined equation:

$$\omega_0 t_r = \frac{\pi}{2} - 3\arcsin(\frac{2}{\pi}\omega_0 t_0 - 1) \tag{7}$$

During propagation, the electron was accelerated thereby obtaining kinetic energy. The electron releases energy in the form of a photon upon recombination with the core. The energy of photon is a combination of the ionization potential of the atom and the accumulated kinetic energy:

$$\hbar\omega = I_p + \frac{1}{2} m_e v^2(t_r) = I_p + 2U_p(\sin(\omega_0 t_r) - \sin(\omega_0 t_0))^2 \tag{8}$$

with U_p being the ponderomotive energy and defined by:

$$U_p = \frac{E_0^2}{4\omega_0^2} \tag{9}$$

By combining equation 7 and 8, the emitted photon energy can be written in terms of times of ionization by using equation 7

$$\hbar\omega = I_p + 2U_p \left(\cos\left(3\arcsin\left(\frac{2}{\pi}\omega_0 t_0 - 1 \right) \right) - \sin(\omega_0 t_0) \right)^2 \tag{10}$$

From this expression the maximum photon can be calculated as:

$$\hbar\omega_{\max} = I_p + 3.17 U_p \tag{11}$$

3 Methods

3.1 Sample Preparation

All the samples were dropcasted onto a 7.5 mm by 7.5 mm piece of quartz. Prior to dropcasting, the quartz was placed in a beaker with acetone and sonicated for 10 minutes to remove contaminations that might be attached to the quartz. Subsequently the piece of quartz was placed onto a heating plate at roughly 100°C to evaporate the remaining isopropanol.

Sodium salicylate samples were prepared by dropcasting a 180 mg/mL sodium salicylate in methanol solution onto the substrate until a white layer is formed. The carbazole benzoic acid samples were prepared by dropcasting a 10 mg/mL 4CB in chloroform solution onto the substrate until a white layer is formed. Non substituted zirconium oxo clusters were prepared by dissolving 10 mg $Zr_4O_2(OMc)_{12}$ in 1 mL of a 9:1 v/v mixture of chloroform and propylene glycol methyl ether acetate (PGMEA). ZrOxo Clusters substituted with 4CB were prepared by mixing 9.5 mg $Zr_4O_2(OMc)_{12}$ and 1.9 mg 4CB (1:1 mol ratio) in 1 mL of a 9:1 v/v mixture of chloroform and (PGMEA). This results in an equilibrium mixture containing primarily single substituted ZrOxo clusters. Double substituted ZrOxo clusters were obtained by preparing the same mixture with twice the amount of 4CB.

For all samples, the quartz was left on the heating plate at 90°C while the solution was being dropcasted onto the quartz and left for 5 minutes to evaporate the solvent. This method yielded a complete coverage of the quartz with a thickness of several 100 μm.

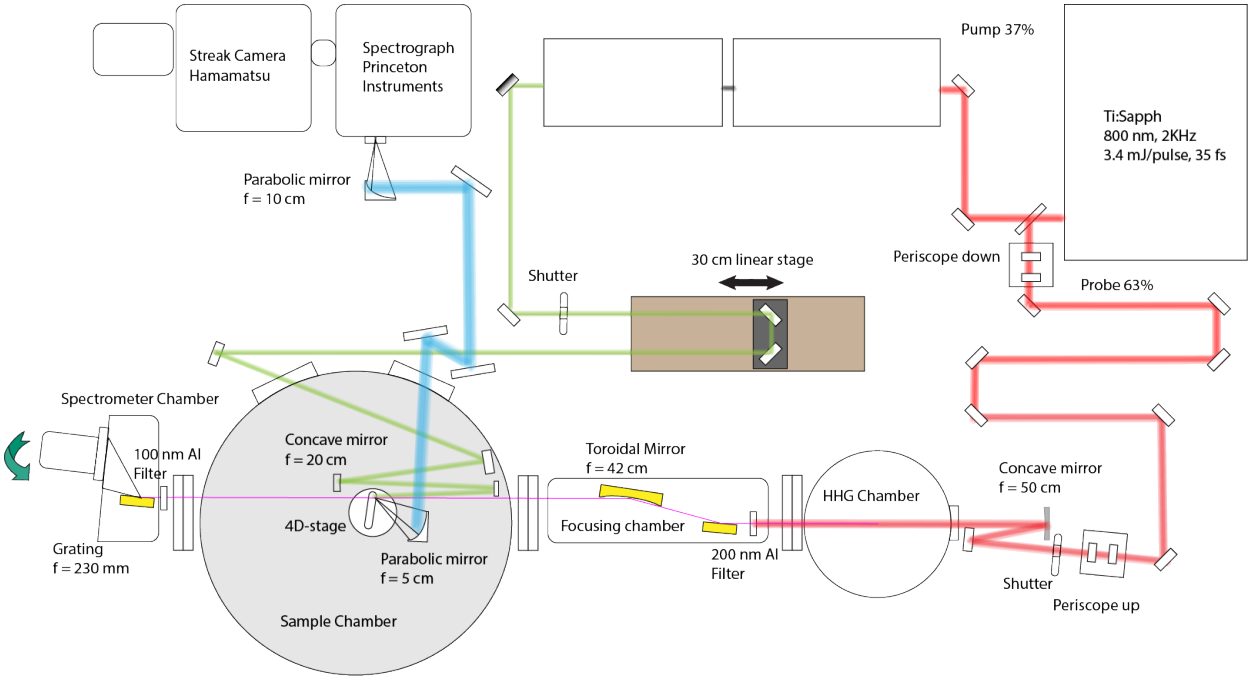

Figure 4: Schematic overview of the tabletop HHG set-up with possibilities to perform XEOL and TAS measurements.

3.2 Experimental Setup

The setup that is used is a tabletop setup which is suitable for high harmonic generation, solid state and liquid fluorescence measurements as well as pump probe measurements. The graphical scheme of the setup can be seen in figure 4. A Titanium:Sapphire laser (Solstice ACE, Spectra-Physics) is used to generate 800nm, 3.4 mJ, 35 fs pulses with a frequency of 2 kHz. The output beam is split with a ratio of 37:63 by a beamsplitter. The 63% is directed towards the HHG chamber and the 37% is directed into an OPA system (TOPAS-Prime, Light Con-version). The OPA system is connected to a compartment which holds multiple nonlinear crystals and high reflectors. With the OPA system and the extra compartment, wavelengths between 240 nm and 2500 nm can be generated with an energy between 0.02 mJ and 0.6 mJ per pulse, respectively. The energy per pulse fluctuates significantly with the wavelength, however the energy per pulse for UV is generally less than for IR. The output is directed into the monster chamber. In the path to the monster chamber, a delay stage is incorporated which can alter the delay by 2 ns with an accuracy of 1.2 fs[29]. Inside the monster chamber, the beam is focused such that the beam overlaps with the beam from the HHG chamber. The beam after the beamsplitter that is directed towards the HHG chamber is send through multiple optics before entering the HHG chamber. To also generate the even harmonics, the second harmonic of the 800 nm beam can be generated by a barium borate (BBO) crystal. The fundamental beam and the second harmonic are temporally overlapped by a calcite crystal and the polarization is aligned by a half-wave plate. Subsequently the beam containing the fundamental beam and the second harmonic are focused into a gas cell containing a generating gas medium in the HHG chamber. A typical HHG spectrum that is generated can be observed in figure 5A. The beam containing the high harmonics extending deep into the XUV are filtered through a 200 nm aluminium filter to remove the 800 and 400 nm from the beam. A gold coated toroidal mirror focuses the beam into the monster chamber. The beam coming from the OPA is used to pump the sample and the beam from the HHG chamber is used to probe the sample. The probe beam can be send through a 100 nm aluminium filter and onto an aberration-corrected flat-field XUV-grating (1200 l/mm,f=235mm, angle of incidence 3 deg, Hamamatsu). The spectrally dispersed beam is send onto an XUV sensitized charge-coupled device (CCD) camera (GreatEyes).

Both the pump and probe beam can also be used for luminescence measurements by directing the beam onto a sample in the monster chamber. The luminescence is collected by a parabolic mirror (f=5cm) and send outside the monster chamber and via DUV enhanced aluminium mirrors directed towards the streak camera (Hamamatsu). Another parabolic mirror (f=10cm) is used to focus the beam into the spectrograph that is connected to the streak camera. The pump beam can also be redirected to a sample stage outside the monster chamber, from which the luminescence is collected and sent into the spectrograph and streak camera. A typical streak measurements can be observed in figure 5B

3.3 Fitting Models

The obtained time and wavelength resolved luminescence spectra have been fitted with the programming software MATLAB. The emission wavelength of the luminescence can be determined by integrating over the time axis and subsequently fitting the spectrum with a Gaussian function. This is only possible if the luminescence is Gaussian and not when has a

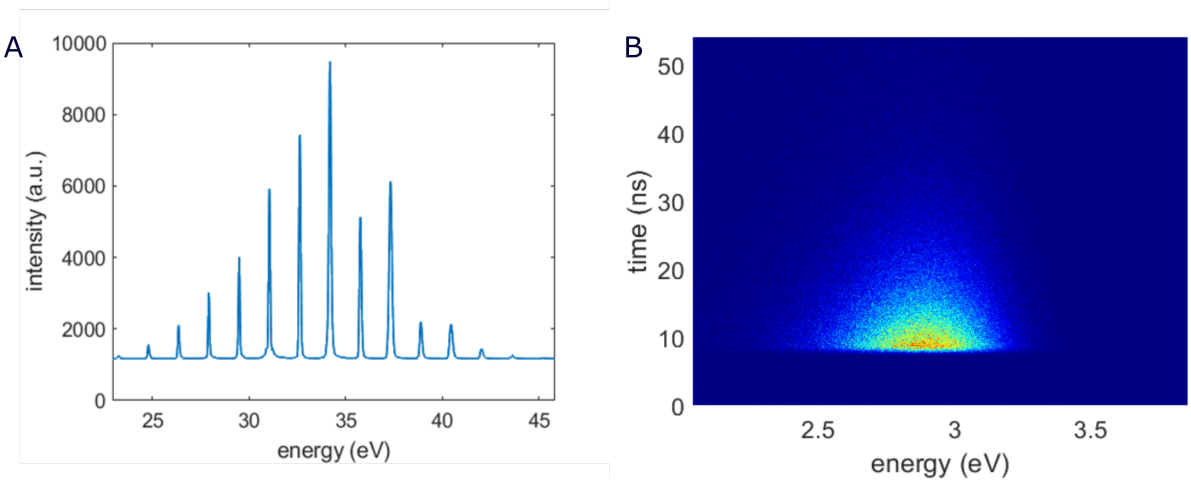

Figure 5: (A) A typical HHG spectrum obtained by generation in argon with a pulsed 800 nm laser. Each peak corresponds to a distinct harmonic of the fundamental 800 nm beam. (B) A typical streak measurement

tail extending into higher or lower energies.

$$I(\lambda) = \frac{A}{\sigma\sqrt{2\pi}} * \exp\left(-\frac{\lambda - \lambda_0}{2\sigma^2}\right) \tag{12}$$

The time dependence of the luminescence can be determined by integrating of the wavelength axis and subsequently fitting the spectrum with an exponentially decreasing function convoluted with the error function indicated the start of the luminescence.[30] The exponential function can be a single exponential function or a multiple exponential function depending on the physical nature of the luminescence. The error function is a result of the Heaviside function convoluted with the system response which is described by a Gaussian function. When a single function does not suffice to fit the spectrum properly, for instance due to exchange between the luminescent state and a dark state [31] or the presence of multiple luminescent species, a sum of functions previously described can be used as the fitting function.

$$I(t) = \frac{A}{2} * \exp\left(-\left(\frac{t - t_0}{\tau} - \frac{\sigma^2}{2\tau}\right)\right) * \left(1 + \operatorname{erf}\left(\frac{(t - t_0) - \sigma^2/\tau}{\sigma\sqrt{2}}\right)\right) \tag{13}$$

It is also possible to fit wavelength axis and time axis of the recorded streak trace simultaneously. This has the advantage that in the presence of two luminescent species, the emission wavelengths and decay times of the individual species can be determined. This can be achieved by multiplication of the Gaussian function of the emission wavelength with the exponential function of the decay.

$$I(\lambda, t) = \frac{A}{\sigma\sqrt{2\pi}} * \exp\left(-\frac{\lambda - \lambda_0}{2\sigma^2}\right) * \exp\left(-\left(\frac{t - t_0}{\tau} - \frac{\sigma^2}{2\tau}\right)\right) * \left(1 + \operatorname{erf}\left(\frac{(t - t_0) - \sigma^2/\tau}{\sigma\sqrt{2}}\right)\right) \tag{14}$$

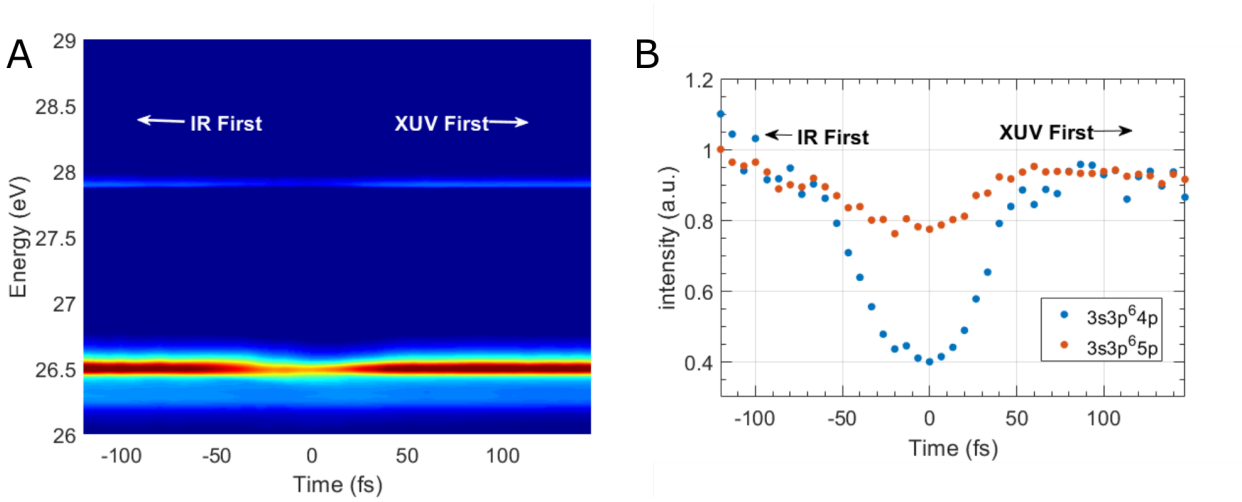

Figure 6: (A) The harmonics signal as a function of energy and delay time between the pump and the probe pulse. (B) The intensity of the 17^{th} (blue) and 18^{th} (red) harmonic as a function of delay between the pump and the probe pulse.

4 Results and Discussion

4.1 Transient Absorption

The focus on this report is on XEOL to investigate ultrafast processes, yet TAS measurements have also been performed. Since the results are still interesting they will be briefly discussed.

To find the exact time that the pump and probe beams are overlapped, t_0, a measurement was performed in which both beams were sent into a gas cell with argon in the monster chamber. The probe beam was set to 860 nm and an output power of 90 μJ/pulse. Argon has 3 transitions which coincide with the energy of the 17^{th}, 18^{th} and 19^{th} harmonic of 800 nm (26.35 eV, 27.90 eV and 29.45 eV, respectively). The corresponding transitions are $3s^23p^6$ to $3s3p^64p$, $3s^23p^6$ to $3s3p^65p$ and $3s^2p^6$ to $3s3p^66p$, respectively. In the absence of a NIR field the argon atoms excited by the XUV pulse will exponentially decay to Ar^+. In the presence of a NIR field, this decay is accelerated and will result in more absorption of the harmonics and therefore a decrease will be observed in the intensity of the corresponding harmonics. Wang et. al. has shown that this effect is most clear for the first two transitions, observing a drop of 20%-40% and 40%-60% respectively depending on the strength of the NIR laser. Therefore the signal of the 17^{th} and 18^{th} harmonic is recorded with the CCD camera. Figure 6 shows the intensity of the 17^{th} and 18^{th} harmonic. A clear decrease in the intensity of the harmonics can be observed as a function of time delay between the pump and probe pulse. The decrease in intensity seems symmetric in the positive and negative part of the delay, this is due to the stretching of the pulse in the TOPAS. The experiments performed by Wang et. al. utilized a 5 fs pulse and they have shown that the decrease is asymmetric. So the time resolution is limited by the NIR pulse length.

4.2 XUV Excited Optical Luminescence

With XUV excited optical luminescence, the time scales of internal conversion and charge transfer have been investigated. Measurements on sodium salicylate and 4CB have been

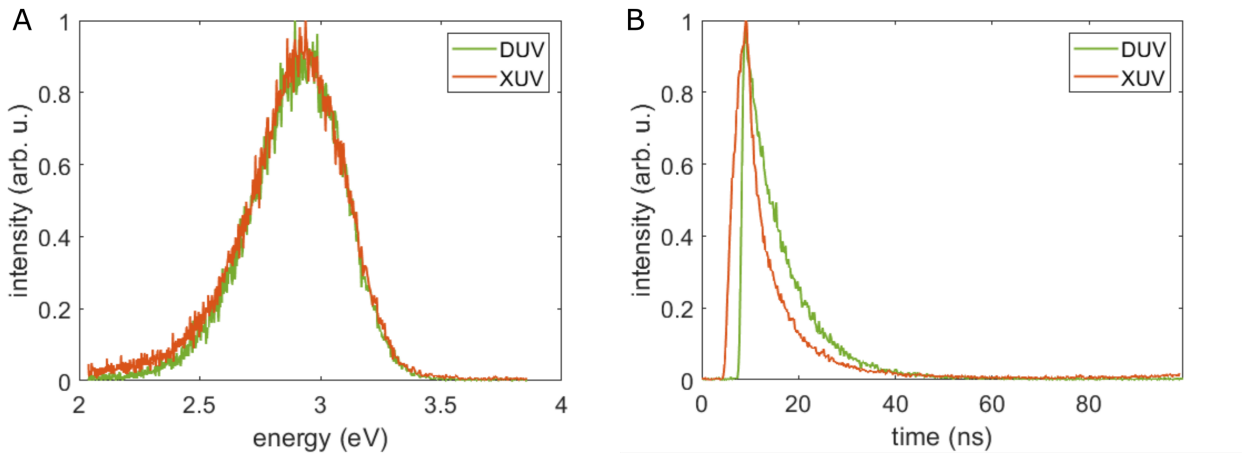

Figure 7: (A) Emission spectrum and (B) time-resolved luminescence of sodium salicylate under DUV (green) and XUV excitation (orange)

performed to reveal information about internal conversion. To investigate the charge transfer timescales, measurements on a zirconium based photoresist material have been performed. The photoresist is a zirconium oxo cluster stabilized with 12 methacrylate (OMc) ligands ($Zr_4O_2(OMc)_{12}$) and the same zirconium oxo cluster with one and two of the OMc ligands substituted with a 4CB molecule. ($Zr_4O_2(OMc)_{12-x}(4CB)_x$).

4.2.1 Internal Conversion

Figure 7A shows the time integrated spectrum of DUV and XUV excited luminescence of sodium salicylate, respectively. The DUV excited luminescence has its maximum at 2.9 eV which is similar to what is found in literature. The luminescence wavelength does not shift

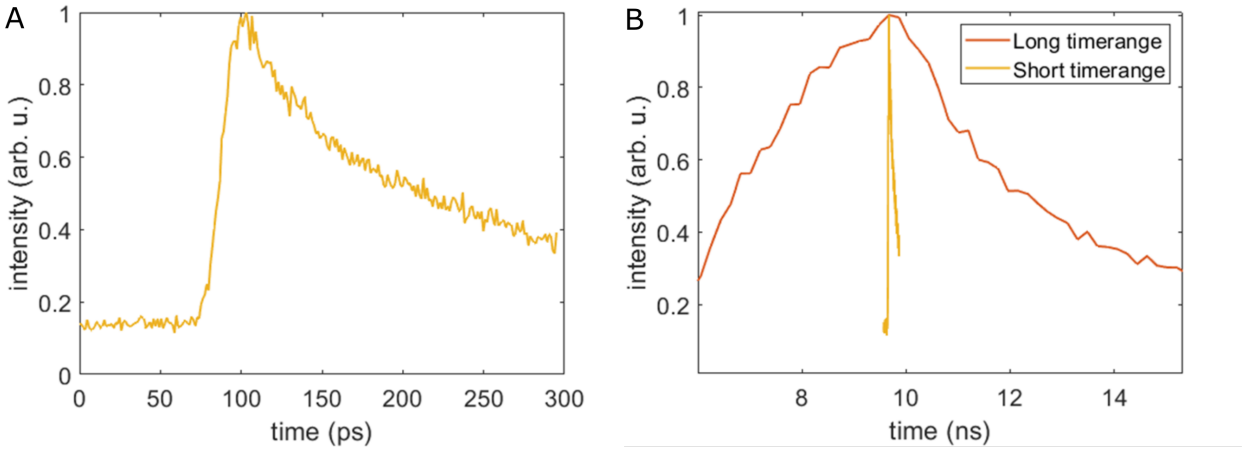

Figure 8: (A) Time-dependent luminescence intensity of XUV excited sodium salicylate on a 300 ps time range and (B) a comparison of the time-resolved XUV excited luminescence measurements on a 300 ps time range (yellow) and a 100 ns time range (orange). The maxima are overlapped and a zoom-in is made to better compare the measurements on the 300 ps time range with the measurements on the 100 ns time range.

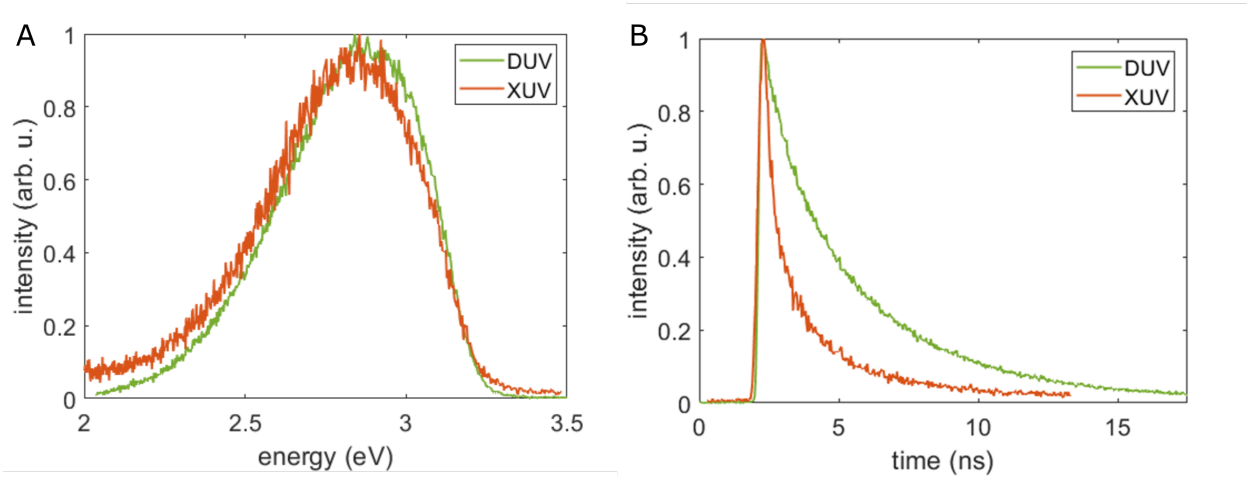

Figure 9: (A) Emission spectrum and (B) time-resolved luminescence of 4CB under DUV (green) and XUV (orange) excitation

upon XUV excitation. This is expected because the luminescent transition is not dependent on the excitation wavelength.[32] The corresponding decay traces are shown in figure 7B. The decay of the DUV excited luminescence is fitted with a single exponentially decaying function as given in equation 13 and gives a decay time of 7.72 $\pm$ 0.04 ns. The measured decay time is in accordance with previous literature.[16] As opposed to the similar emission spectra, the decay trace of the XUV excited luminescence is significantly different. It can no longer be properly fitted with a mono-exponential decay and is therefore fitted with a bi-exponential decay with $\tau_1 = 1.18 \pm 0.09$ ns and $\tau_2 = 7.08 \pm 0.45$ ns. The relative amplitudes of the two components are $A_1 = 0.72$ and $A_2 = 0.28$ a.u.. It also seems that the rise time of the XUV excited luminescence is significantly longer than for the DUV excited luminescence. This is not suspected to be real, but caused by the difference in how the measurements are performed. Between the spectrograph and the streak camera is a manual slit with which the intensity of the luminescence that enters the streak camera can be regulated. The XUV excited luminescence is much weaker than the DUV excited luminescence, therefore the manual slit is opened more than with the DUV excited luminescence. This results in a broader system response and therefore results in a broader apparent rise time.

Previous experiments with the streak camera have indicated that the system response is around one percent of the time range of the measurement. The aforementioned measurements were with a 100 ns time range, this means that the system response is around 1 ns. The fast decay time of 1.18 ns is likely resolution limited and actually faster. Therefore measurements have been performed with a 300 ps time range (figure 8A). This luminescence trace was fitted with a bi-exponential decay where the slow decay of 7.08 ns was fixed because that would not be resolved with such a short time range. The fast decay constant obtained in this time range was 68 $\pm$ 4 ps. This shows that the system response has a major impact in unveiling sub nanoseconds decay constants. Figure 8B shows the decay traces of the 300 ps time range and 100 ns time range measurements. This shows that the actual luminescence decays significantly faster than initially measured at a long time range which is caused by the system response.

A mechanism has been proposed Brocklehurst and coworkers in 1997. The 68 ps lifetime is attributed to the luminescent transition which is accelerated due to quenching by the

charged environment. The charged environment is a result of the high energetic XUV photons which ionizes the material. The slower decay, 7.08 ns is attributed to an additional excited state which replenishes the luminescent state.[33] This suggests that there is a slow route from the highly excited states to the HOMO resulting with a lifetime of 7.08 ns and a fast route which causes the initial population of the LUMO and thereby the instantaneous luminescence intensity. To confirm whether the 68 ps lifetime is indeed due to charge quenching, measurements have to be performed in the 300 ps, or shorter, time range with varying flux of the excitation beam. More XUV photons will result in more ionization and therefore more charge quenching.

Figure 9 shows the results of the luminescence of 4CB under excitation of light with a wavelength of 266 nm. The luminescence has its maximum at 2.9 eV and has a long tail extending to lower energies. The luminescence decay seems intrinsically bi-exponential and is therefore fitted with a bi-exponential decay with $\tau_1 = 4.26 \pm 0.07$ ns and $\tau_2 = 1.08 \pm 0.06$ ns and relative amplitudes $A_1 = 0.64$ a.u. and $A_2 = 0.36$ a.u.. XUV excitation again results in the same emission spectrum and a faster decay with decay constants $\tau_1 = 3.26 \pm 0.23$ ns and $\tau_2 = 0.51 \pm 0.04$ ns and amplitudes $A_1 = 0.23$ a.u. and $A_2 = 0.77$ a.u.. The faster decay constants are again on the order of the system response and are therefore likely resolution limited. Both decay constants are accelerated, but the relative amplitudes reversed. With DUV excitation, the slower decay constant had a higher amplitude than the faster decay whereas in XUV excitation this is the other way around. This can again indicate that charge quenching plays a role. However, the physical origin of the intrinsic bi-exponential decay of 4CB is unknown and therefore concrete conclusions cannot be drawn.

4.2.2 Charge Transfer

The following results should be read with precaution. Prior experiments indicated that the zirconium methacrylate oxo cluster, henceforth referred to as ZrOxo cluster, showed no luminescence in the visible range. Contrary to the prior experiments, the results that will be discussed here show that the ZrOxo cluster shows luminescence in the visible range. This luminescence resembles the luminescence of 4CB, but redshifted and therefore the ZrOxo clusters are suspected to be contaminated or hydrolysed. This has not yet been confirmed or denied and therefore the results will be presented.

The results of the experiments on the ZrOxo clusters are shown in figure 10, orange curve. The maximum of the emission is at 2.7 eV. The decay trace is fitted with a bi-exponential decay with time constants of 6.79 ± 0.13 ns and 1.09 ± 0.11 ns, with relative amplitudes of 0.53 a.u. and 0.47 a.u..

Substituting a methacrylate ligand in ZrOxo clusters with a 4CB ligand results in a spectrum and decay that closely resembles the spectrum and decay of the ZrOxo cluster without 4CB. Incorporation of the 4CB also results in an enhancement of the luminescence intensity. The luminescence of the ZrOxo clusters without 4CB was barely visible, whereas the luminescence of the ZrOxo clusters with 4CB was clearly visible. Figure 10 shows the results of the 4CB, ZrOxo without 4CB, ZrOxo with 1 4CB substituted and ZrOxo with 2 4CB substituted. The emission spectrum shows that the luminescence of $ZrOxo(OMc)_{12-x}(4CB)_x$ is red shifted from 2.9 to 2.7 eV compared to the luminescence of 4CB. The decay times of single and double substituted ZrOxo clusters are also comparable to non substituted ZrOxo clusters, $\tau_1 = 6.67 \pm 0.37$ns and $\tau_2 = 1.53 \pm 0.19$ ns with relative amplitudes $A_1 = 0.61$ a.u. and $A_2 = 0.39$ a.u. and $\tau_1 = 6.65 \pm 0.11$ ns and $\tau_2 = 1.25 \pm 0.07$ ns with relative

amplitudes $A_1 = 0.61$ a.u and $A_2 = 0.39$ a.u., respectively. Taking a closer look at the start of the luminescence, the rise, seems to show that the non substituted ZrOxo clusters take longer to reach the maximum of the luminescence. This would imply that the incorporation of the 4CB enhances the rate at which the luminescent state is populated. As previously mentioned, the luminescence from the non substituted ZrOxo clusters was much weaker than the substituted ZrOxo clusters. Therefore, the manual slit is also opened more resulting in a broader system response.

These results show that 4CB is not the luminescent species when incorporated into the ZrOxo cluster. Multiple arguments are presented that indicate that the carbazole ligand is excited followed by charge transfer to the ZrOxo cluster. (1) The non substituted ZrOxo clusters showed very weak luminescence while the luminescence of 4CB was clearly visible. (2) The emission of single and double substituted ZrOxo clusters is close to the emission wavelength as non substituted ZrOxo clusters, which is different from the emission wavelength of 4CB. (3) The decay rates of single and double substituted ZrOxo clusters are comparable to the decay rate of non substituted ZrOxo clusters whereas the decay rate of 4CB is significantly faster. These arguments suggest that the 4CB is excited and the charge is transferred to the ZrOxo cluster where the luminescence happens.

5 Conclusion

In conclusion, extreme ultra-violet (XUV) excited optical luminescence measurements using a tabletop set-up and high harmonic generation as the XUV source has shown to be capable of measuring on the picosecond timescale. It has been shown that the results are dependent on the time range of the measurements. Therefore, to investigate processes in the picosecond range, the measurements have to be performed on the picosecond time range. Investigating processes that are sub-picosecond require a time range of a few picoseconds or less. This is achievable with the current system, but requires further optimization.

The aim of XUV excited optical luminescence was to investigate time scales of internal conversion and charge transfer. The timescales of these processes are in the range of

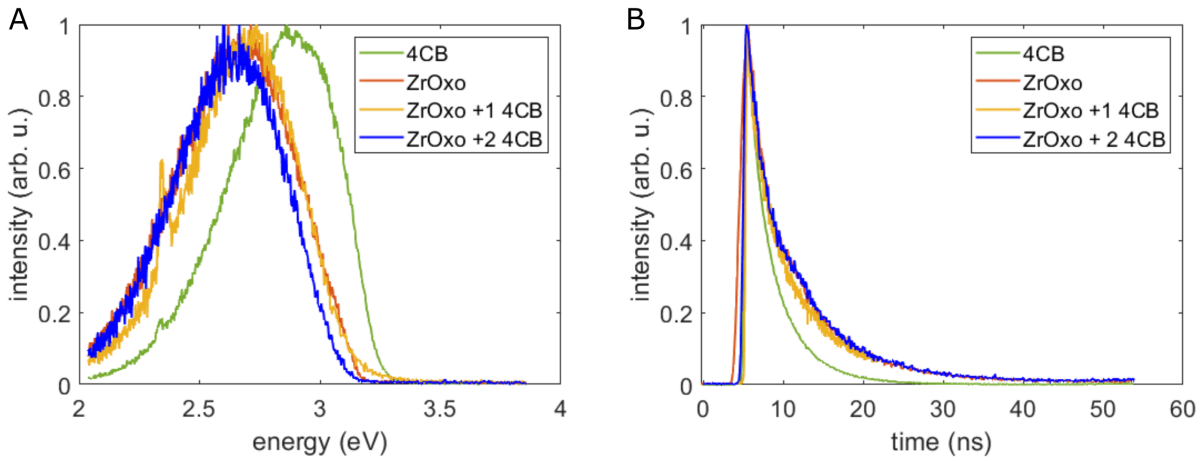

Figure 10: (A) Emission spectrum and (B) time-resolved luminescence of 4CB (green), Non substituted ZrOxo cluster (orange), single substituted (yellow) and double substituted (blue) ZrOxo cluster under DUV excitation

picosecond to attosecond. Due to the need to further optimize the measurements, this has not been succeeded. Measurements have been performed in the picosecond to nanosecond time range to investigate the difference between DUV and XUV excited luminescence of sodium salicylate and carbazole benzoic acid. Measurements have also been performed on the charge transfer process of carbazole benzoic acid (4CB) and a zirconium based photoresist, zirconium oxo clusters.

Comparing DUV excited luminescence with XUV excited luminescence showed that the luminescence spectrum did not change. This is as expected by Kasha's rule, the luminescent transition is independent of the excitation energy. The observed luminescence decay is accelerated upon XUV excitation as compared to DUV excitation. This is attributed to quenching due to the charged environment. For sodium salicylate, the luminescent decay is accelerated to 68 ps as a result of quenching. The XUV excited luminescence decay of sodium salicylate also revealed a decay constant of 7.1 ns which is attributed to replenishing of the LUMO by a long lived excited state.

The measurements on 4CB, zirconium oxo clusters and zirconium oxo cluster with 4CB ligands revealed that the luminescence originates from the zirconium oxo cluster. The luminescence of single and double substituted zirconium oxo clusters resembles the luminescence of non substituted zirconium oxo clusters instead of the luminescence of 4CB. This is also observed in the decay rates. 4CB has a bi-exponential decay with time constants 4.26 ns and 1.08 ns while substituted and non substituted zirconium oxo clusters has a bi-exponential decay with decay constants of around 6.7 ns and 1.2 ns. The decay constants of around 1 ns are assumed to be resolution limited due to the system response. These results have indicated that the charge is transferred to the zirconium oxo clusters instead of to the 4CB.

6 Outlook

The results described in this report do not conclude the research towards the internal conversion and charge transfer timescales. Although the system is capable of performing measurements on the picosecond timescale, investigation of the rise time has not succeeded. In order to investigate the rise time, optimization of the streak measurements on the tens of picosecond timescale is required. Besides optimization of the measurements, a more thorough investigation of the materials is interesting. The proposed luminescence mechanism of sodium salicylate is not confirmed and can be investigated. This can be achieved by quantum mechanical calculations and checking whether the quenching of the luminescence is dependent on the intensity of the excitation pulse. Quantum mechanical calculations can also give insight into the luminescence mechanism of 4CB and reveal the origin of the intrinsic bi-exponential decay. For the charge transfer measurements it is possible to use a ligand that has a higher fluorescence wavelength, lower fluorescence energy, than the zirconium oxo cluster. This can have the effect that the lowest lying luminescent state is on the ligand instead of on the zirconium oxo cluster thereby resulting in luminescence originating from the ligand.

References

[1] P. B. Corkum. Plasma perspective on strong field multiphoton ionization. *PRL*, 71(13):1994–1997, September 1993.

[2] P. M. Kraus and H. J. Wörner. Attosecond nuclear dynamics in the ammonia cation: Relation between high-harmonic and photoelectron spectroscopies. *ChemPhysChem*, 14(7):1445–1450, April 2013.

[3] P. B. Corkum and Ferenc Krausz. Attosecond science. *Nature Physics*, 3(6):381–387, June 2007.

[4] T. Gaumnitz, A. Jain, Y. Pertot, M. Huppert, I. Jordan, F. Ardana-Lamas, and H. J. Wörner. Streaking of 43-attosecond soft-X-ray pulses generated by a passively CEP-stable mid-infrared driver. *Opt. Express*, 25(22):27506–27518, October 2017.

[5] M. Schultze, E. M. Bothschafter, A. Sommer, S. Holzner, W. Schweinberger, M. Fiess, M. Hofstetter, R. Kienberger, V. Apalkov, V. S. Yakovlev, M. I. Stockman, and F. Krausz. Controlling dielectrics with the electric field of light. *Nature*, 493(7430):75–78, January 2013.

[6] A. Rogalev and J. Goulon. *Chemical Applications of Synchrotron Radiation*, chapter 15 - X-RAY EXCITED OPTICAL LUMINESCENCE SPECTROSCOPIES, pages 707–760. 2002.

[7] A. N. Belsky, A. N. Vasil'ev, V. V. Mikhailin, A. V. Gektin, N. V. Shiran, A. L. Rogalev, and E. I. Zinin. Time-resolved XEOL spectroscopy of new scintillators based on CsI. *Review of Scientific Instruments*, 63(1):806–809, June 1992.

[8] A. Moulet, J. B. Bertrand, T. Klostermann, A. Guggenmos, N. Karpowicz, and E. Goulielmakis. Soft x-ray excitonics. *Science*, 357(6356):1134, September 2017.

[9] T. Sekikawa, T. Ohno, Y. Nabekawa, and S. Watanabe. Auger-free luminescence excited by high-order harmonics of a femtosecond Ti:sapphire laser. *Journal of Luminescence*, 87-89:827 – 829, 2000.

[10] T. Shimizu, T.and Sekikawa, T. Kanai, S. Watanabe, and M. Itoh. Time-Resolved Auger Decay in CsBr Using High Harmonics. *PRL*, 91(1):017401, July 2003.

[11] H. J. Wörner, C. A. Arrell, N. Banerji, A. Cannizzo, M. Chergui, A. K. Das, P. Hamm, U. Keller, P. M. Kraus, E. Liberatore, P. Lopez-Tarifa, M.o Lucchini, M. Meuwly, C. Milne, J.-E. Moser, U. Rothlisberger, G. Smolentsev, J. Teuscher, J. A. van Bokhoven, and O. Wenger. Charge migration and charge transfer in molecular systems. *Structural Dynamics*, 4(6):061508, May 2017.

[12] K. Kise, H. Watanabe, K. Itoga, H. Sumitani, and M. Amemiya. Improvement of resolution in x-ray lithography by reducing secondary electron blur. *Journal of Vacuum Science & Technology B: Microelectronics and Nanometer Structures Processing, Measurement, and Phenomena*, 22(1):126–130, June 2020.

[13] P. M. Kraus and H. J. Wörner. Perspectives of Attosecond Spectroscopy for the Understanding of Fundamental Electron Correlations. *Angew. Chem. Int. Ed.*, 57(19):5228–5247, April 2018.

[14] J. W. Thackeray, M. Wagner, S. J. Kang, and J. Biafore. Understanding the Role of Acid vs. Electron Blur in EUV Resist Materials. *Journal of Photopolymer Science and Technology*, 23(5):631–637, 2010.

[15] F. E. Williams and L. Marton. Solid-State Luminescence. In *Advances in Electronics and Electron Physics*, volume 5, pages 137–168. Academic Press, January 1953.

[16] H. C. Joshi, H. Mishra, and H. B. Tripathi. Photophysics and photochemistry of salicylic acid revisited. *Journal of Photochemistry and Photobiology A: Chemistry*, 105(1):15–20, May 1997.

[17] R. S. Sigmond. Ultra-violet pulse response of sodium salicylate. *British Journal of Applied Physics*, 17(10):1307–1312, October 1966.

[18] N. Kristianpoller and R. A. Knapp. Some Optical Properties of Sodium Salicylate Films. *Applied Optics*, 3(8):915–918, August 1964.

[19] V. Kumar and A. K. Datta. Vacuum ultraviolet scintillators: sodium salicylate and p-terphenyl. *Applied Optics*, 18(9):1414–1417, May 1979.

[20] J. A. R. Samson. Vacuum ultraviolet research. *Applied Optics*, 6(3):403–408, March 1967.

[21] F. Masuda, M. Kochi, S. Iwashima, and H. Inokuchi. Intensity Measurements in Vacuum Ultraviolet Region by Aromatic Phosphors. *Japanese Journal of Applied Physics*, 6(12):1423–1426, December 1967.

[22] G. J. Baker, B. Brocklehurst, and I. R. Holton. Time dependence of sodium salicylate luminescence excited by VUV photons, X-rays and β particles: magnetic field effects. *Journal of Physics B: Atomic and Molecular Physics*, 20(10):L305–L310, May 1987.

[23] P. Xie, N. Yuan, S. Li, Y. Ouyang, Y. Zhu, and H. Liang. Synthesis and properties of blue luminescent bipolar materials constructed with carbazole and anthracene units with 4-cyanophenyl substitute at the 9-position of the carbazole unit. *Luminescence*, 33(3):604–610, May 2020.

[24] H. Shao, X. Chen, Z. Wang, and P. Lu. Synthesis and fluorescence properties of carbazole and fluorene-based compounds. *Journal of Luminescence*, 127(2):349–354, December 2007.

[25] L. Wu, M. Vockenhuber, Y. Ekinci, and S. Castellanos. The role of the organic shell in hybrid molecular materials for EUV lithography. In *Extreme Ultraviolet (EUV) Lithography X*, volume 10957, March 2019.

[26] J. J. Yeh and I. Lindau. Atomic subshell photoionization cross sections and asymmetry parameters: $1 \leq Z \leq 103$. *Atomic Data and Nuclear Data Tables*, 32(1):1–155, January 1985.

[27] H. Chen, Y. Tang, T. Jiang, G. Li, D. L. Andrews, R. H. Lipson, and T. Nann. Nonlinear Nanophotonics With 2D Transition Metal Dichalcogenides. In *Comprehensive Nanoscience and Nanotechnology (Second Edition)*, pages 305–318. Academic Press, Oxford, January 2019.

[28] M. Ferray, A. L'Huillier, X. F. Li, L. A. Lompre, G. Mainfray, and C. Manus. Multiple-harmonic conversion of 1064 nm radiation in rare gases. *Journal of Physics B: Atomic, Molecular and Optical Physics*, 21(3):L31–L35, February 1988.

[29] M. van der Geest, N. Sadegh, T. M. Meerwijk, E. I. Wooning, L. Wu, A. M. Brouwer, and P. M. Kraus. Time- and Frequency Resolved Luminescence using an Ultrafast Table-Top Extreme Ultraviolet Source. 2020, In Preparation.

[30] B. J. Selby, T. I. Quickenden, and C. G. Freeman. The Fitting of Luminescence Rises and Decays. *Kinetics and Catalysis*, 44(1):5–15, January 2003.

[31] A. J. Goodman, A. P. Willard, and W. A. Tisdale. Exciton trapping is responsible for the long apparent lifetime in acid-treated mos_2. *PRB*, 96(12):121404, September 2017.

[32] M. Kasha. Characterization of electronic transitions in complex molecules. *Discuss. Faraday Soc.*, 9(0):14–19, 1950.

[33] B. Brocklehurst. Spin correlation and magnetic field effects in radiolysis. *Radiation Physics and Chemistry*, 50(3):213–225, September 1997.